Engineering Artificial Atomic Systems of Giant Electric Dipole Moment

Baiyi Yu,[1] Yaoming Chu,[1,*] Ralf Betzholz,[1] Shaoliang Zhang,[1,†] and Jianming Cai[1,2,3,‡]
[1]School of Physics, International Joint Laboratory on Quantum Sensing and Quantum Metrology, Hubei Key Laboratory of Gravitation and Quantum Physics, Institute for Quantum Science and Engineering, Wuhan National High Magnetic Field Center, Huazhong University of Science and Technology, Wuhan 430074, China
[2]Shanghai Key Laboratory of Magnetic Resonance, East China Normal University, Shanghai 200062, China
[3]Wuhan Institute of Quantum Technology, Wuhan, Hubei 430074, China

(Received 1 May 2023; revised 6 July 2023; accepted 22 January 2024; published 16 February 2024)

The electric dipole moment (EDM) plays a crucial role in determining the interaction strength of an atom with electric fields, making it paramount to quantum technologies based on coherent atomic control. We propose a scheme for engineering the potential in a Paul trap to realize a two-level quantum system with a giant EDM formed by the motional states of a trapped electron. We show that, under realistic experimental conditions, our system exhibits enhanced EDMs compared to those attainable with Rydberg atoms, serving as a complementary counterpart in the megahertz (MHz) resonance-frequency range. Furthermore, we show that such artificial atomic dipoles can be efficiently initialized, read out, and coherently controlled, thereby providing a potential platform for quantum technologies such as ultrahigh-sensitivity electric-field sensing.

DOI: 10.1103/PhysRevLett.132.073202

Introduction.—Coherent coupling between atoms and electromagnetic fields is one of the most essential ingredients in light-matter interactions. The magnetic dipole of quantum systems allows using the magnetic field gradients to couple the electron's spin to its motion [1–5], while the electric coupling strength critically depends on the magnitude of the electric dipole moment (EDM) of the atomic system [6,7]. A large EDM, and thereby a strong coupling, significantly enhances the speed of coherent manipulation [8], enables novel driving or coupling regimes [9–32], and increases the sensitivity to electric fields [33–36]. For example, the large EDM endows Rydberg atoms with exceptional sensitivity to electric fields [37–44] and the resulting strong interatomic dipole-dipole interaction already successfully shows great promise for applications in quantum information processing [45–53]. In ^{87}Rb atoms, for instance, the EDM between neighboring states with the principal quantum number $n \sim 65$ is roughly $4000ea_0$, with the elementary charge e and Bohr radius a_0, which corresponds to 0.2 eμm [37].

In Rydberg atoms, further augmenting the EDM by increasing the principal quantum number would result in small binding energies ($\propto n^{-2}$) [47,54] and thereby instability of the Rydberg states. This corresponds to the case if the transition frequency were to reach the MHz range, a range that is indispensable in broadcasting and air-to-ground communication, owing to the long wavelengths and extended propagation distances [41–44]. Therefore, it would be appealing to realize an alternative controllable system with giant EDMs as a complement to Rydberg atoms in the MHz resonance-frequency range.

In this Letter, we systematically engineer the trapping potential for a single electron to obtain a two-level quantum system, formed by Rydberg-like motional states of the electron, with a resonance frequency within the MHz range and an EDM of several eμm. The engineered potential bears the essential feature of the Coulomb potential in natural atoms, i.e., the inverse-distance form, and more importantly ensures the stability of the eigenstates with giant EDMs. We show that the system can be initialized via fast quasiadiabatic dynamics by appropriately deforming the potential [55–58]. Under realistic experimental conditions, our analysis demonstrates that the EDM can reach 7 eμm, more than an order of magnitude larger than those between stable Rydberg states, with initialization and readout fidelities above 95%. We demonstrate that recent progress in trapping and controlling electrons in Paul traps [59–62] suggests the feasibility of the scheme we present and that the system may provide a superior performance in electric-field sensing.

Anharmonic potential engineering.—Our goal is to construct a stable two-level system with a giant EDM by designing a suitable trapping potential. Figure 1(a) shows the prototype of our trap, which combines two symmetric layers of electrodes separated along the y direction. The ac electrodes [red in Fig. 1(a)] are driven by a radio-frequency (rf) voltage, generating effective confinement in the radial (x and y) directions with a secular frequency ω_r (see Supplemental Material (SM) [63], Sec. I B). The key element in our design is the extension of the potential generated by the dc electrodes [blue and yellow in Fig. 1(a)] from merely second order, as in usual Paul traps [60–62,80–82], to third, fourth, or even higher order in the axial coordinate z. In Fig. 1(b), the yellow line shows the actual potential Φ_{3D} generated by the dc electrodes along

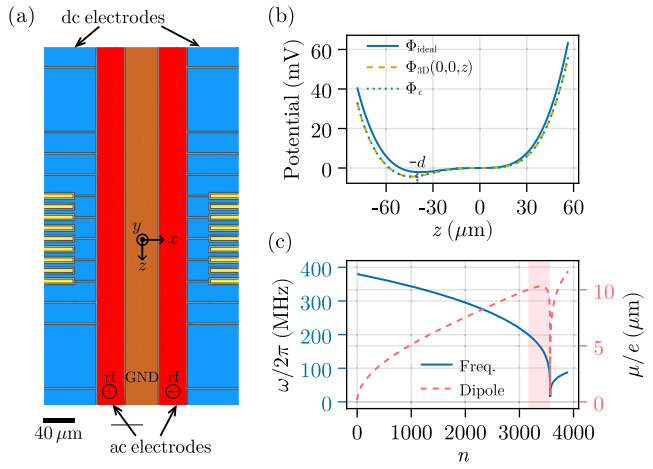

FIG. 1. (a) Cropped geometry of the electrodes in our trap design (see SM [63], Sec. I A for a more detailed geometry). The ac electrodes (red) are driven by the same rf voltage but with opposite phase, whereas the dc electrodes (blue and yellow) are supplied with voltages symmetric around the z axis. (b) Φ_{ideal} is the ideal potential of the form $a_2z^2 + a_3z^3 + a_4z^4$, Φ_{3D} is the actual potential generated by the dc-electrode design, and Φ_c is the effective axial potential obtained from Eq. (2). (c) Transition frequency (blue) and the corresponding EDM (red) between the eigenstates $|\psi_{n+1}\rangle$ and $|\psi_n\rangle$ for the effective axial potential Φ_c shown in (b). The pink region covers quantum numbers with $3156 \leq n \leq 3565$. For (b) and (c), we have used the parameters $d = 40$ μm and $\omega_h' = (2\pi)300$ MHz.

$x = y = 0$. The most significant component of the potential has the form $a_2z^2 + a_3z^3 + a_4z^4$ along $x = y = 0$, as shown by the blue line. The coefficients a_3 and a_4 have the form (see SM [63], Sec. I C)

$$a_3 = \frac{2a_2'}{3d}, \qquad a_4 = \frac{3a_3}{4d}, \tag{1}$$

where d represents the distance between the two points along axis z satisfying $\partial(a_3z^3 + a_4z^4)/\partial z = 0$ and $a_2' = m_e\omega_h'^2/2e$ describes the approximately harmonic confinement of $a_3z^3 + a_4z^4$ around $z = -d$ with frequency ω_h'. Without loss of generality, we choose the parameters $d = 40$ μm and $\omega_h' = (2\pi)300$ MHz for numerical demonstrations.

This results in a potential similar to the Coulomb potential over a certain range of z. We calculate the eigenenergies and eigenstates of the axial-motion Hamiltonian $H_z = p_z^2/2m_e + e\Phi_c(z)$, where $\Phi_c(z)$ is the effective axial potential

$$\Phi_c(z) = \iint (\Phi_{3D} + \Phi_{pp})|\psi(x)|^2|\psi(y)|^2 dxdy, \tag{2}$$

with $\psi(x)$ and $\psi(y)$ representing the electron wave function in the x and y direction, respectively, and Φ_{pp} denoting the

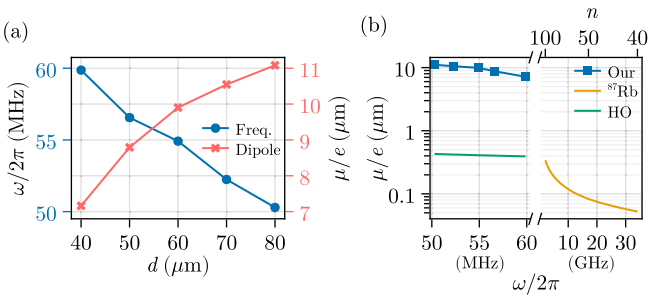

FIG. 2. (a) Dependence of the transition frequency and the EDM on the potential parameter d, which is obtained by using the actual effective potentials with $\omega_h' = (2\pi)300$ MHz. (b) EDM as a function of the transition frequency. Blue: two-level systems from our design. Yellow: Rydberg states $(n + 1)P_{3/2}m_j = 1/2$ and $nD_{5/2}m_j = 1/2$ of ^{87}Rb [37,40] with n in the range 40–100 (calculated using the Alkali Rydberg Calculator package [83]). Green: harmonic-oscillator ground state and single-phonon Fock state.

static rf pseudopotential. We note that the effective potential [cf. Eq. (2)] agrees well with the actual potential, as shown in Fig. 1(b), and accounts for the axial-radial motion couplings induced by the third-, fourth-, and higher-order dc-potential terms, and the imperfections of both the dc and rf potentials arising from realistic experimental conditions; see SM [63], Sec. I D.

In Fig. 1(c), the blue line shows the transition frequency between the eigenstates $|\psi_{n+1}\rangle$ and $|\psi_n\rangle$, of the axial-motion Hamiltonian H_z, and the red line shows the corresponding EDM, which exceeds 10 eμm within the pink region with highly nonlinear eigenenergies. Here, the EDM between the ith and jth eigenstates, $|\psi_i\rangle$ and $|\psi_j\rangle$, of the z-direction motion is defined as

$$\mu_{ij} = e\langle\psi_i|z|\psi_j\rangle. \tag{3}$$

In contrast to Rydberg states, these large-quantum-number eigenstates are still stably trapped in the designed potential. In Fig. 2(a), we show that the EDM increases for a larger d, whereas the transition frequency decreases (see SM [63], Sec. III). A comparison between Rydberg states, harmonic-oscillator Fock states, and the eigenstates of our system is shown in Fig. 2(b). The result demonstrates that our platform would be appealing for quantum applications in the MHz frequency range, where the EDMs promised by our proposal are more than an order of magnitude larger than those achieved by stable Rydberg states with the principal quantum number $n < 100$ and harmonic-oscillator Fock states.

System initialization.—We proceed to demonstrate that the two-level system formed by the neighboring motional eigenstates with giant EDMs can be efficiently initialized by a potential deformation [84]. Initially, the electron is trapped in a standard Paul trap with an axial harmonic

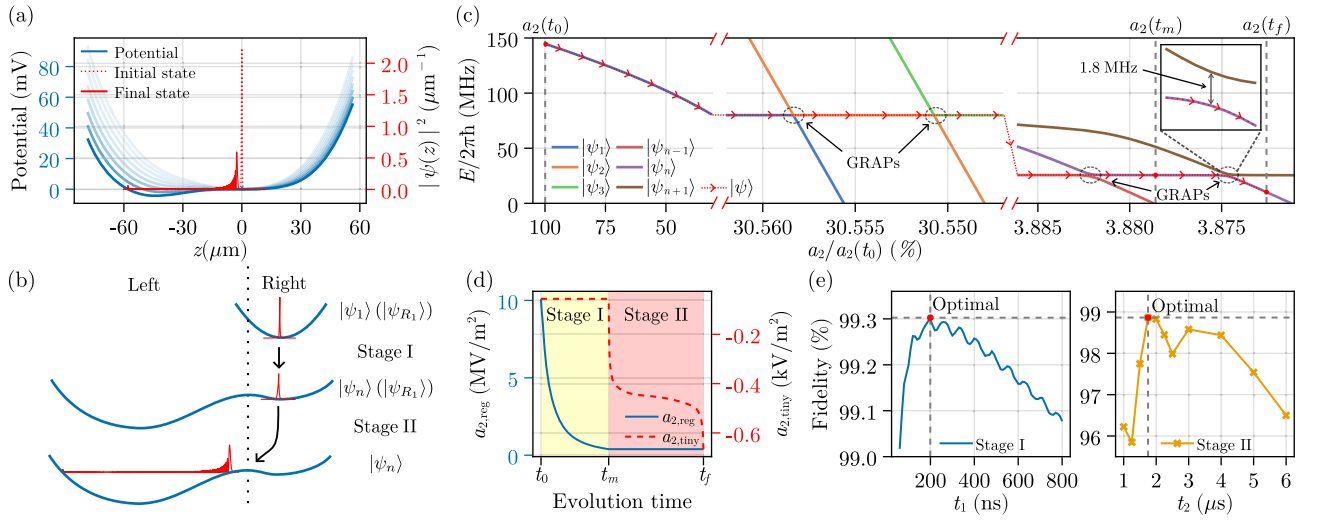

FIG. 3. (a) Potential deformation from the light blue into the deep blue curve. The initial state depicted by the dotted red line is the ground state of the initial potential, whereas the final state depicted by the solid red line is the 3566th eigenstate of the final potential. (b) Illustration of the evolution throughout the different stages, where $|\psi_{R_1}\rangle$ is the ground state of the right well and $|\psi_j\rangle$ is the jth eigenstate of the full potential. (c) Eigenenergies for the eigenstates of the full potential as a function of a_2, presenting the ideal trajectory of $|\psi\rangle$ in the a_2 parameter space, for example, with $n = 3566$. (e) Fidelity between the ideal eigenstate and the prepared state after Stage I and Stage II as a function of the evolution time of the two stages, which is obtained from numerical simulation. The right panel of (e) is obtained with an optimal Stage-I evolution time $t_1 = 199.4$ ns.

potential $a_2 z^2$, where $a_2 = m_e \omega_z^2/2e$ corresponds to a trap frequency of $\omega_z = (2\pi)300$ MHz. It is then brought close to the motional ground state using the cooling techniques developed in other related systems [59,85–87] (see Sec. II A in SM [63]). Subsequently, applying additional voltages to the blue dc electrodes, the higher order terms of the potential shown in Fig. 1(b) is added. The electron is approximately in the ground state of the new potential, since the higher order contributions are negligible compared to the initial harmonic potential. The parameter a_2 is then gradually decreased to deform the effective axial potential, as shown in Fig. 3(a), from the lightest blue curve to the deepest blue one [i.e., the green dotted line shown in Fig. 1(b)]. Meanwhile, the system evolves into the nth eigenstate of the designed potential, which is a component of our two-level system.

The evolution of the state $|\psi\rangle$ can be divided into two distinct stages, as shown in Fig. 3(b). Stage I (from t_0 to t_m) transforms the state $|\psi\rangle$ from the initial harmonic-potential ground state $|\psi_1\rangle$ into the nth eigenstate $|\psi_n\rangle$ of the full potential. During this stage, the evolution is adiabatic only when a_2 is away from GRAPs. Here, the acronym GRAP stands for energy-level anticrossing point (abbreviated as AP) in a_2 parameter space [see Fig. 3(c)] of a state initially approximating the ground state of the right well (abbreviated as GR). At these GRAPs, the state $|\psi\rangle$ nonadiabatically crosses energy levels, resulting in an increment of the quantum number [88,89]. We remark that the large detuning between axial and radial modes will suppress the possible axial-radial phonon leakage at corresponding anticrossings. When the anticrossing gaps at the GRAPs are small, Stage I can be approximated by an adiabatic decrease of the right-well confinement and a fast quasiadiabatic method [57] can be utilized to speed up the process. Thus, the trajectory of a_2 during Stage I obeys

$$\frac{da_2}{dt} = -\frac{\epsilon}{\hbar}\min_{i\neq 1}\left|\frac{[E_{R_1}(a_2) - E_{R_i}(a_2)]^2}{\langle\psi_{R_1}(a_2)|\frac{\partial H}{\partial a_2}|\psi_{R_i}(a_2)\rangle}\right|, \tag{4}$$

where $\epsilon \ll 1$ is a constant and $E_{R_i}(a_2)$ and $|\psi_{R_i}(a_2)\rangle$ are the ith instantaneous eigenvalue and eigenstate, respectively, of the right well for a specific a_2. Assuming the right well is nearly harmonic, this trajectory reads (see SM [63], Sec. II C)

$$a_2(t) = \left[4\sqrt{e/m_e}\epsilon t + \sqrt{1/a_2(t_0)}\right]^{-2}. \tag{5}$$

Stage II (from t_m to t_f) is an adiabatic process, during which the trajectory of a_2 can also be calculated by an equation similar to Eq. (4). An example trajectory is shown in Fig. 3(d) with $a_2(t_0)$, $a_2(t_m)$, and $a_2(t_f)$ indicated by vertical dashed lines in Fig. 3(c). The resulting anticrossing gap between $a_2(t_m)$ and $a_2(t_f)$ is $(2\pi)1.8$ MHz. The final two-level system, in this example, is composed of $|\psi_n\rangle$ and $|\psi_{n-1}\rangle$ with $n = 3566$, possessing a transition frequency of $(2\pi)59.9$ MHz and an EDM of 7.16 $e\mu$m.

To precisely control the potential deformation during the two stages, we decompose $a_2 z^2$ into two parts, namely $a_{2,\mathrm{reg}} z^2$ and $a_{2,\mathrm{tiny}} z^2$, generated by the blue and yellow dc electrodes, respectively [cf. Fig. 1(a)]. Because of the small size and the specific placement of the yellow dc electrodes,

the voltages supplied to the yellow ones are of the same magnitude as those supplied to the blue ones even if $a_{2,\mathrm{tiny}}$ is orders of magnitude smaller than $a_{2,\mathrm{reg}}$ (see SM [63], Sec. I E). In Fig. 3(e), we show the fidelity between the ideal eigenstate $|\psi_n\rangle$ and the actually prepared three-dimensional state $|\psi_{3\mathrm{D}}\rangle$ after Stage I (Stage II) as a function of the evolution time $t_1 = t_m - t_0$ ($t_2 = t_f - t_m$), which is defined as

$$F = \langle\psi_{3\mathrm{D}}|(I_x \otimes I_y \otimes |\psi_n\rangle\langle\psi_n|)|\psi_{3\mathrm{D}}\rangle, \tag{6}$$

with the identity operators I_x and I_y of the motion in the x and y dimensions, respectively. The left panel of Fig. 3(e) demonstrates an optimal evolution time of Stage I, which balances the competing effects that necessitate fast potential deformation near GRAPs and slow deformation elsewhere. The right panel of Fig. 3(e) is likewise obtained with this optimal $t_1 = 199.4$ ns, showing that the initialization fidelity can reach 98.8% for $t_2 = 1.75$ μs (see SM [63], Secs. II D, II E).

State readout.—For the state readout of the two-level system formed by eigenstates $|\psi_n\rangle$ and $|\psi_{n'}\rangle$ of H_z, we first transfer the information of the motional states onto the spin degree of freedom of the trapped electron using a magnetic-field gradient oscillating with the frequency ω_B that is resonant with the transition of the two-level system. This is described by the Hamiltonian

$$H_B = H_z - \mu_{\mathrm{B}} b_y s_y z \cos(\omega_B t + \phi_B), \tag{7}$$

with the Bohr magneton μ_{B}, the y Pauli matrix s_y of the spin degree of freedom, and $b_y = \partial B_y/\partial z$. On the other hand, we denote the x and y Pauli operators of the motional two-level system by σ_x and σ_y, respectively. In the interaction picture with respect to H_z, one can perform a rotating-wave approximation and thereby obtain (see SM [63], Sec. IV A)

$$H_B^{(\mathrm{int})} = -\frac{1}{2}\hbar g s_y \otimes \sigma_\phi, \tag{8}$$

where $\sigma_\phi = \cos(\phi)\sigma_x + \sin(\phi)\sigma_y$, $\phi = \phi_B - \phi_z$, with $\phi_z = \arg(z_{nn'})$, $z_{nn'} = \langle\psi_n|z|\psi_{n'}\rangle$, and $g = \mu_{\mathrm{B}} b_y |z_{nn'}|/\hbar$. Hamiltonian (8) induces a conditional rotation of the spin state. If the spin is initialized into the state $|\uparrow\rangle$ (the $+1$ eigenstate of s_z), after $t = \pi/2g$, the spin state will have been rotated into $|+\rangle$ or $|-\rangle$ (namely the ± 1 eigenstates of s_x), depending on the motional-state projection on the eigenstates of σ_ϕ, i.e., $|\downarrow_\phi\rangle$ or $|\uparrow_\phi\rangle$. Therefore, the information on the motional states is transformed into the populations of the spin eigenstates of s_x, which can then be read out through a spin measurement based on developed techniques in Paul and Penning traps [59,80,85,90–93].

We proceed to numerically simulate this transfer process and calculate the average fidelity $F_{\mathrm{avg}} = (F_+ + F_-)/2$, where $F_\pm$ represents the fidelity between the final spin state and the ideal state $|\pm\rangle$ for the initial motional states $|\downarrow_\phi\rangle$ and $|\uparrow_\phi\rangle$, respectively. The influence of electric-field noise is explicitly taken into account by employing a master equation (see SM [63], Sec. IV B), where the noise-induced transition rate between the eigenstates is specified by the spectral density of the noise. Figure 4(a) shows how the average fidelity changes with the spin-motion coupling strength g. If the coupling is too strong to ensure the validity of the rotating-wave approximation, the averaged fidelity would be very low. On the other hand, if the coupling is too weak, the averaged fidelity will also decrease due to the action of the noise over the long transfer time $\pi/2g$. As shown in Fig. 4(a), the average fidelity can reach 95.2% for an optimal transfer time of 180 ns, which, thanks to the large EDM, only requires a magnetic-field gradient $b_y = 14$ T/m that is experimentally feasible [1–5].

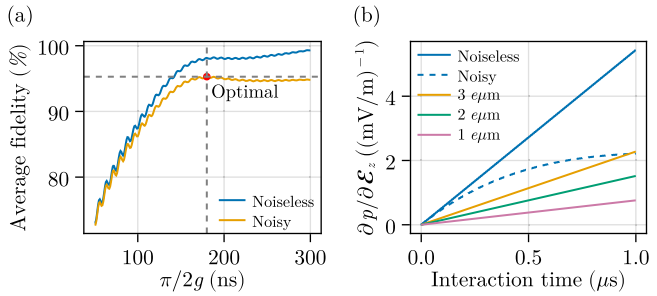

FIG. 4. (a) Average readout fidelity as a function of the transfer time $\pi/2g$, which is obtained from numerical simulation in the Hilbert space composed by the spin space and the motional subspace formed by the eigenstates $|\psi_{3561}\rangle$ through $|\psi_{3575}\rangle$ of the potential with $a_2(t_f)$ from Fig. 3(c) (see SM [63], Sec. IV C). (b) Susceptibility $\partial p/\partial \mathcal{E}_z|_{\mathcal{E}_z=0}$ as a function of the interaction time for an EDM of 7.16 eμm without (solid blue) and with noise (dashed blue), which is compared with the noiseless results for the EDMs of 1 (pink), 2 (green), and 3 eμm (yellow). In both (a) and (b), we assume the spectral density of the electric-field noise to follow the power law $S_E(\omega) \propto 1/\omega^{1.3}$ with $S_E[(2\pi)1\ \mathrm{MHz}] \approx 10^{-12}\ (\mathrm{V/m})^2/\mathrm{Hz}$ for a 4-K environment and a particle-surface distance of 30 μm [94,95].

Coherent control and quantum sensing.—Owing to the nonlinear eigenenergies, the artificial atomic dipoles can be coherently controlled as a two-level system by an oscillating electric field along the axial direction with amplitude $\mathcal{E}_z$, frequency ω_E, and phase ϕ_E. This can be described by the Hamiltonian

$$H_E = H_z - ez\mathcal{E}_z \cos(\omega_E t + \phi_E). \tag{9}$$

To characterize how fast the two-level system formed by $|\psi_n\rangle$ and $|\psi_{n'}\rangle$ can be controlled, we introduce the effective detuning

$$\Delta\omega_{nn'} = \min_{i\in(n,n'),j\notin(n,n')} \left(\frac{|\mu_{nn'}|}{|\mu_{ij}|}\Delta\omega_{ij,nn'}\right), \tag{10}$$

where $\Delta\omega_{ij,nn'} = ||\omega_{ij}| - |\omega_{nn'}||$ with $\omega_{ij} = (E_i - E_j)/\hbar$. The coherent-control Rabi frequency $\Omega_R = |\mu_{nn'}|\mathcal{E}_z/\hbar$ is required to be much smaller than the effective detuning to ensure that leakage to other energy levels is negligible (see SM [63], Sec. IV A). For $a_2(t_f)$ from Fig. 3(c), one finds an effective detuning of $(2\pi)5.5$ MHz (see SM [63], Sec. II B).

Lastly, in the same framework, we consider the quantum sensing of a weak electric field along the axial direction that is oscillating on resonance with the transition of the two-level system, i.e., with the frequency $\omega_E = \omega_{nn'}$. The system is initialized into $|\psi_n\rangle$, and after an interaction time t, the probability to find the system in the $+1$ eigenstate of σ_ϕ, with $\phi = \phi_E - \phi_z - \pi/2$, reads $p = [1 + \sin(\Omega_R t)]/2$ (see SM [63], Sec. IV A). Taking into account the influence of the electric-field noise, the susceptibility of this probability to the electric-field strength can be written as $(\partial p/\partial\mathcal{E}_z)|_{\mathcal{E}_z=0} = |\mu_{nn'}| \exp(-\Gamma t)t/2\hbar$, where Γ is an effective decay rate (see SM [63], Sec. IV C). Figure 4(b) demonstrates that, even in a noisy environment, the giant-EDM sensor presents an improved susceptibility in a certain range of the interaction time, indicating an enhanced metrological performance [96].

Conclusion.—We have presented a novel method to create a two-level system with a giant EDM, formed by motional states of an electron confined in a specially engineered Paul trap. In order to show the practicality of the proposal, we have presented the efficient initialization and readout, as well as the coherent manipulation of the system, with consideration of realistic experimental conditions. Our detailed analysis and numerical simulations demonstrate the feasibility of our approach within state-of-the-art experimental capabilities. Furthermore, we have illustrated a simple protocol for electric-field sensing, showcasing a very prominent susceptibility to the electric-field strength. Our work represents a promising approach to creating giant EDMs in artificial quantum systems and opens appealing possibilities for coherent atomic control and quantum technologies. The design principles of our approach could potentially be extended to other trapped-electron systems. Typical examples are helium- or neon-trapped electrons [97–100], where the ground-state cooling of single trapped electrons has been demonstrated. In addition, we remark that the present system with giant EDM may offer a possible way to significantly promote coherent interaction between charged particles through conductor wiring [101,102].

This work is supported by the National Natural Science Foundation of China (Grants No. 12161141011 and No. 12174138), the National Key R&D Program of China (Grant No. 2018YFA0306600), and the Shanghai Key Laboratory of Magnetic Resonance (East China Normal University). Y.-M. C. is also supported by the Young Scientists Fund of the National Natural Science Foundation of China (Grant No. 12304572) and the fellowship of China Postdoctoral Science Foundation (Grant No. 2022M721256). Part of the computation was completed on the HPC Platform of Huazhong University of Science and Technology.

*yaomingchu@hust.edu.cn
†shaoliang@hust.edu.cn
‡jianmingcai@hust.edu.cn

[1] C. Ospelkaus, U. Warring, Y. Colombe, K. R. Brown, J. M. Amini, D. Leibfried, and D. J. Wineland, Microwave quantum logic gates for trapped ions, Nature (London) **476**, 181 (2011).
[2] T. P. Harty, M. A. Sepiol, D. T. C. Allcock, C. J. Ballance, J. E. Tarlton, and D. M. Lucas, High-fidelity trapped-ion quantum logic using near-field microwaves, Phys. Rev. Lett. **117**, 140501 (2016).
[3] G. Zarantonello, H. Hahn, J. Morgner, M. Schulte, A. Bautista-Salvador, R. F. Werner, K. Hammerer, and C. Ospelkaus, Robust and resource-efficient microwave near-field entangling $^9Be^+$ gate, Phys. Rev. Lett. **123**, 260503 (2019).
[4] R. Srinivas, S. C. Burd, R. T. Sutherland, A. C. Wilson, D. J. Wineland, D. Leibfried, D. T. C. Allcock, and D. H. Slichter, Trapped-ion spin-motion coupling with microwaves and a near-motional oscillating magnetic field gradient, Phys. Rev. Lett. **122**, 163201 (2019).
[5] R. Srinivas, S. C. Burd, H. M. Knaack, R. T. Sutherland, A. Kwiatkowski, S. Glancy, E. Knill, D. J. Wineland, D. Leibfried, A. C. Wilson, D. T. C. Allcock, and D. H. Slichter, High-fidelity laser-free universal control of trapped ion qubits, Nature (London) **597**, 209 (2021).
[6] M. O. Scully and M. S. Zubairy, *Quantum Optics* (Cambridge University Press, Cambridge, England, 1997).
[7] *Quantum Optics*, edited by D. F. Walls and G. J. Milburn (Springer, Berlin, Heidelberg, 2008).
[8] M. Saffman, T. G. Walker, and K. Mølmer, Quantum information with Rydberg atoms, Rev. Mod. Phys. **82**, 2313 (2010).
[9] W. D. Oliver, Y. Yu, J. C. Lee, K. K. Berggren, L. S. Levitov, and T. P. Orlando, Mach-Zehnder interferometry in a strongly driven superconducting qubit, Science **310**, 1653 (2005).
[10] M. Silveri, J. Tuorila, M. Kemppainen, and E. Thuneberg, Probe spectroscopy of quasienergy states, Phys. Rev. B **87**, 134505 (2013).
[11] A. Barfuss, J. Teissier, E. Neu, A. Nunnenkamp, and P. Maletinsky, Strong mechanical driving of a single electron spin, Nat. Phys. **11**, 820 (2015).
[12] K. Jiménez-García, L. J. LeBlanc, R. A. Williams, M. C. Beeler, C. Qu, M. Gong, C. Zhang, and I. B. Spielman, Tunable spin-orbit coupling via strong driving in ultracold-atom systems, Phys. Rev. Lett. **114**, 125301 (2015).
[13] K. R. K. Rao and D. Suter, Nonlinear dynamics of a two-level system of a single spin driven beyond the rotating-wave approximation, Phys. Rev. A **95**, 053804 (2017).

[14] Y. Yan, Z. Lü, J. Y. Luo, and H. Zheng, Effects of counter-rotating couplings of the Rabi model with frequency modulation, Phys. Rev. A **96**, 033802 (2017).

[15] W. L. Yang, W. L. Song, J.-H. An, M. Feng, D. Suter, and J. Du, Floquet engineering to entanglement protection of distant nitrogen vacancy centers, New J. Phys. **21**, 013007 (2019).

[16] M. Brune, F. Schmidt-Kaler, A. Maali, J. Dreyer, E. Hagley, J. M. Raimond, and S. Haroche, Quantum Rabi oscillation: A direct test of field quantization in a cavity, Phys. Rev. Lett. **76**, 1800 (1996).

[17] S. D. Hogan, J. A. Agner, F. Merkt, T. Thiele, S. Filipp, and A. Wallraff, Driving Rydberg-Rydberg transitions from a coplanar microwave waveguide, Phys. Rev. Lett. **108**, 063004 (2012).

[18] A. A. Morgan and S. D. Hogan, Coupling Rydberg atoms to microwave fields in a superconducting coplanar waveguide resonator, Phys. Rev. Lett. **124**, 193604 (2020).

[19] P. Forn-Díaz, L. Lamata, E. Rico, J. Kono, and E. Solano, Ultrastrong coupling regimes of light-matter interaction, Rev. Mod. Phys. **91**, 025005 (2019).

[20] A. Frisk Kockum, A. Miranowicz, S. De Liberato, S. Savasta, and F. Nori, Ultrastrong coupling between light and matter, Nat. Rev. Phys. **1**, 19 (2019).

[21] Y. Tokura, W. G. van der Wiel, T. Obata, and S. Tarucha, Coherent single electron spin control in a slanting Zeeman field, Phys. Rev. Lett. **96**, 047202 (2006).

[22] A. Cottet and T. Kontos, Spin quantum bit with ferromagnetic contacts for circuit QED, Phys. Rev. Lett. **105**, 160502 (2010).

[23] K. D. Petersson, L. W. McFaul, M. D. Schroer, M. Jung, J. M. Taylor, A. A. Houck, and J. R. Petta, Circuit quantum electrodynamics with a spin qubit, Nature (London) **490**, 380 (2012).

[24] T. Frey, P. J. Leek, M. Beck, A. Blais, T. Ihn, K. Ensslin, and A. Wallraff, Dipole coupling of a double quantum dot to a microwave resonator, Phys. Rev. Lett. **108**, 046807 (2012).

[25] E. Kawakami, P. Scarlino, D. R. Ward, F. R. Braakman, D. E. Savage, M. G. Lagally, M. Friesen, S. N. Coppersmith, M. A. Eriksson, and L. M. K. Vandersypen, Electrical control of a long-lived spin qubit in a Si/SiGe quantum dot, Nat. Nanotechnol. **9**, 666 (2014).

[26] J. J. Viennot, M. C. Dartiailh, A. Cottet, and T. Kontos, Coherent coupling of a single spin to microwave cavity photons, Science **349**, 408 (2015).

[27] F. Beaudoin, D. Lachance-Quirion, W. A. Coish, and M. Pioro-Ladrière, Coupling a single electron spin to a microwave resonator: Controlling transverse and longitudinal couplings, Nanotechnology **27**, 464003 (2016).

[28] X. Mi, J. V. Cady, D. M. Zajac, P. W. Deelman, and J. R. Petta, Strong coupling of a single electron in silicon to a microwave photon, Science **355**, 156 (2017).

[29] A. J. Landig, J. V. Koski, P. Scarlino, U. C. Mendes, A. Blais, C. Reichl, W. Wegscheider, A. Wallraff, K. Ensslin, and T. Ihn, Coherent spin–photon coupling using a resonant exchange qubit, Nature (London) **560**, 179 (2018).

[30] X. Mi, M. Benito, S. Putz, D. M. Zajac, J. M. Taylor, G. Burkard, and J. R. Petta, A coherent spin-photon interface in silicon, Nature (London) **555**, 599 (2018).

[31] N. Samkharadze, G. Zheng, N. Kalhor, D. Brousse, A. Sammak, U. C. Mendes, A. Blais, G. Scappucci, and L. M. K. Vandersypen, Strong spin-photon coupling in silicon, Science **359**, 1123 (2018).

[32] P. Scarlino, J. H. Ungerer, D. J. van Woerkom, M. Mancini, P. Stano, C. Müller, A. J. Landig, J. V. Koski, C. Reichl, W. Wegscheider, T. Ihn, K. Ensslin, and A. Wallraff, In situ tuning of the electric-dipole strength of a double-dot charge qubit: Charge-noise protection and ultrastrong coupling, Phys. Rev. X **12**, 031004 (2022).

[33] S. Gleyzes, S. Kuhr, C. Guerlin, J. Bernu, S. Deléglise, U. Busk Hoff, M. Brune, J.-M. Raimond, and S. Haroche, Quantum jumps of light recording the birth and death of a photon in a cavity, Nature (London) **446**, 297 (2007).

[34] S. Haroche, Nobel Lecture: Controlling photons in a box and exploring the quantum to classical boundary, Rev. Mod. Phys. **85**, 1083 (2013).

[35] C. L. Degen, F. Reinhard, and P. Cappellaro, Quantum sensing, Rev. Mod. Phys. **89**, 035002 (2017).

[36] M. Zhang, Y. F. Wang, X. Y. Peng, X. N. Feng, S. R. He, Y. F. Li, and L. F. Wei, Sensitive detection of millimeter wave electric field by driving trapped surface-state electrons, arXiv:2304.05154.

[37] J. A. Sedlacek, A. Schwettmann, H. Kübler, R. Löw, T. Pfau, and J. P. Shaffer, Microwave electrometry with Rydberg atoms in a vapour cell using bright atomic resonances, Nat. Phys. **8**, 819 (2012).

[38] A. Osterwalder and F. Merkt, Using high Rydberg states as electric field sensors, Phys. Rev. Lett. **82**, 1831 (1999).

[39] A. Facon, E.-K. Dietsche, D. Grosso, S. Haroche, J.-M. Raimond, M. Brune, and S. Gleyzes, A sensitive electrometer based on a Rydberg atom in a Schrödinger-cat state, Nature (London) **535**, 262 (2016).

[40] M. Jing, Y. Hu, J. Ma, H. Zhang, L. Zhang, L. Xiao, and S. Jia, Atomic superheterodyne receiver based on microwave-dressed Rydberg spectroscopy, Nat. Phys. **16**, 911 (2020).

[41] C. L. Holloway, M. T. Simons, J. A. Gordon, P. F. Wilson, C. M. Cooke, D. A. Anderson, and G. Raithel, Atom-based RF electric field metrology: From self-calibrated measurements to subwavelength and near-field imaging, IEEE Transactions on Electromagnetic Compatibility **59**, 717 (2017).

[42] B. Liu, L.-H. Zhang, Z.-K. Liu, Z.-Y. Zhang, Z.-H. Zhu, W. Gao, G.-C. Guo, D.-S. Ding, and B.-S. Shi, Highly sensitive measurement of a megahertz rf electric field with a Rydberg-atom sensor, Phys. Rev. Appl. **18**, 014045 (2022).

[43] R. C. Brown, B. Kayim, M. A. Viray, A. R. Perry, B. C. Sawyer, and R. Wyllie, Very-high- and ultrahigh-frequency electric-field detection using high angular momentum Rydberg states, Phys. Rev. A **107**, 052605 (2023).

[44] A. P. Rotunno, S. Berweger, N. Prajapati, M. T. Simons, A. B. Artusio-Glimpse, C. L. Holloway, M. Jayaseelan, R. M. Potvliege, and C. S. Adams, Detection of 3–300 MHz electric fields using Floquet sideband gaps by "Rabi matching" dressed Rydberg atoms, J. Appl. Phys. **134**, 134501 (2023).

[45] M. D. Lukin, M. Fleischhauer, R. Cote, L. M. Duan, D. Jaksch, J. I. Cirac, and P. Zoller, Dipole Blockade and quantum information processing in mesoscopic atomic ensembles, Phys. Rev. Lett. **87**, 037901 (2001).
[46] J. Beugnon, C. Tuchendler, H. Marion, A. Gaëtan, Y. Miroshnychenko, Y. R. P. Sortais, A. M. Lance, M. P. A. Jones, G. Messin, A. Browaeys, and P. Grangier, Two-dimensional transport and transfer of a single atomic qubit in optical tweezers, Nat. Phys. **3**, 696 (2007).
[47] D. Comparat and P. Pillet, Dipole blockade in a cold Rydberg atomic sample, J. Opt. Soc. Am. B **27**, A208 (2010).
[48] H. Bernien, S. Schwartz, A. Keesling, H. Levine, A. Omran, H. Pichler, S. Choi, A. S. Zibrov, M. Endres, M. Greiner, V. Vuletić, and M. D. Lukin, Probing many-body dynamics on a 51-atom quantum simulator, Nature (London) **551**, 579 (2017).
[49] A. Keesling, A. Omran, H. Levine, H. Bernien, H. Pichler, S. Choi, R. Samajdar, S. Schwartz, P. Silvi, S. Sachdev, P. Zoller, M. Endres, M. Greiner, V. Vuletić, and M. D. Lukin, Quantum Kibble-Zurek mechanism and critical dynamics on a programmable Rydberg simulator, Nature (London) **568**, 207 (2019).
[50] A. Browaeys and T. Lahaye, Many-body physics with individually controlled Rydberg atoms, Nat. Phys. **16**, 132 (2020).
[51] S. Ebadi, T. T. Wang, H. Levine, A. Keesling, G. Semeghini, A. Omran, D. Bluvstein, R. Samajdar, H. Pichler, W. W. Ho, S. Choi, S. Sachdev, M. Greiner, V. Vuletić, and M. D. Lukin, Quantum phases of matter on a 256-atom programmable quantum simulator, Nature (London) **595**, 227 (2021).
[52] G. Semeghini, H. Levine, A. Keesling, S. Ebadi, T. T. Wang, D. Bluvstein, R. Verresen, H. Pichler, M. Kalinowski, R. Samajdar, A. Omran, S. Sachdev, A. Vishwanath, M. Greiner, V. Vuletić, and M. D. Lukin, Probing topological spin liquids on a programmable quantum simulator, Science **374**, 1242 (2021).
[53] S. J. Evered, D. Bluvstein, M. Kalinowski, S. Ebadi, T. Manovitz, H. Zhou, S. H. Li, A. A. Geim, T. T. Wang, N. Maskara, H. Levine, G. Semeghini, M. Greiner, V. Vuletić, and M. D. Lukin, High-fidelity parallel entangling gates on a neutral-atom quantum computer, Nature (London) **622**, 268 (2023).
[54] T. F. Gallagher, *Rydberg Atoms*, Cambridge Monographs on Atomic, Molecular and Chemical Physics (Cambridge University Press, Cambridge, England, 1994).
[55] S. Martínez-Garaot, E. Torrontegui, X. Chen, M. Modugno, D. Guéry-Odelin, S.-Y. Tseng, and J. G. Muga, Vibrational mode multiplexing of ultracold atoms, Phys. Rev. Lett. **111**, 213001 (2013).
[56] S. Martínez-Garaot, M. Palmero, D. Guéry-Odelin, and J. G. Muga, Fast bias inversion of a double well without residual particle excitation, Phys. Rev. A **92**, 053406 (2015).
[57] S. Martínez-Garaot, A. Ruschhaupt, J. Gillet, T. Busch, and J. G. Muga, Fast quasiadiabatic dynamics, Phys. Rev. A **92**, 043406 (2015).
[58] O. Abah, R. Puebla, and M. Paternostro, Quantum state engineering by shortcuts to adiabaticity in interacting spin-boson systems, Phys. Rev. Lett. **124**, 180401 (2020).
[59] P. Peng, C. Matthiesen, and H. Häffner, Spin readout of trapped electron qubits, Phys. Rev. A **95**, 012312 (2017).
[60] C. Matthiesen, Q. Yu, J. Guo, A. M. Alonso, and H. Häffner, Trapping electrons in a room-temperature microwave Paul trap, Phys. Rev. X **11**, 011019 (2021).
[61] Q. Yu, A. M. Alonso, J. Caminiti, K. M. Beck, R. T. Sutherland, D. Leibfried, K. J. Rodriguez, M. Dhital, B. Hemmerling, and H. Häffner, Feasibility study of quantum computing using trapped electrons, Phys. Rev. A **105**, 022420 (2022).
[62] R. T. Sutherland, Q. Yu, K. M. Beck, and H. Häffner, One- and two-qubit gate infidelities due to motional errors in trapped ions and electrons, Phys. Rev. A **105**, 022437 (2022).
[63] See Supplemental Material at http://link.aps.org/supplemental/10.1103/PhysRevLett.132.073202 for a detailed description of the electrode geometry, derivations of some expressions in this Letter, as well as numerical details on the potential engineering and the simulation of quantum dynamics, which includes Refs. [64–79].
[64] D. Suter and G. A. Álvarez, Colloquium: Protecting quantum information against environmental noise, Rev. Mod. Phys. **88**, 041001 (2016).
[65] J. M. Amini, J. Britton, D. Leibfried, and D. J. Wineland, Microfabricated chip traps for ions, arXiv:0812.3907.
[66] S. Hong, M. Lee, H. Cheon, T. Kim, and D.-i. D. Cho, Guidelines for designing surface ion traps using the boundary element method, Sensors **16**, 616 (2016).
[67] J. D. Jackson, *Classical Electrodynamics* (John Wiley & Sons, Hoboken, 1999).
[68] R. Penrose, On best approximate solutions of linear matrix equations, Math. Proc. Cambridge Philos. Soc. **52**, 17 (1956).
[69] M. Suzuki, Fractal decomposition of exponential operators with applications to many-body theories and Monte Carlo simulations, Phys. Lett. A **146**, 319 (1990).
[70] T. Besard, C. Foket, and B. De Sutter, Effective extensible programming: Unleashing JULIA on GPUs, IEEE Trans. Parallel Distrib. Syst. **30**, 827 (2019).
[71] T. A. Savard, K. M. O'Hara, and J. E. Thomas, Laser-noise-induced heating in far-off resonance optical traps, Phys. Rev. A **56**, R1095 (1997).
[72] S. Krämer, D. Plankensteiner, L. Ostermann, and H. Ritsch, QuantumOptics.jl: A JULIA framework for simulating open quantum systems, Comput. Phys. Commun. **227**, 109 (2018).
[73] C. Rackauckas and Q. Nie, DifferentialEquations.jl—A performant and feature-rich ecosystem for solving differential equations in JULIA, J. Open Res. Software **5**, 15 (2017).
[74] F. C. White, W. Tebbutt, M. Zgubic, Wessel, Rogerluo, N. Robinson, A. Arslan, S. Axen, S. Schaub, D. Widmann, R. Finnegan, A. Robson, B. Richard, C. Vogt, E. Davies, J. E. C. Serrallés, J. TagBot, and V. B. Shah, JULIADiff/FiniteDifferences.jl: v0.12.25, Zenodo (2022), 10.5281/zenodo.7186348.
[75] K. R. Brown, J. Chiaverini, J. M. Sage, and H. Häffner, Materials challenges for trapped-ion quantum computers, Nat. Rev. Mater. **6**, 892 (2021).

[76] A. F. van Driel, G. Allan, C. Delerue, P. Lodahl, W. L. Vos, and D. Vanmaekelbergh, Frequency-dependent spontaneous emission rate from CdSe and CdTe nanocrystals: Influence of dark states, Phys. Rev. Lett. **95**, 236804 (2005).
[77] S. Xu, X. Xia, Q. Yu, S. Khan, E. Megidish, B. You, B. Hemmerling, A. Jayich, J. Biener, and H. Häffner, 3D-printed micro linear Paul trap for scalable quantum information processing, arXiv:2310.00595.
[78] D. J. Wineland and H. G. Dehmelt, Principles of the stored ion calorimeter, J. Appl. Phys. **46**, 919 (1975).
[79] A. Osada, K. Taniguchi, M. Shigefuji, and A. Noguchi, Feasibility study on ground-state cooling and single-phonon readout of trapped electrons using hybrid quantum systems, Phys. Rev. Res. **4**, 033245 (2022).
[80] D. Leibfried, R. Blatt, C. Monroe, and D. Wineland, Quantum dynamics of single trapped ions, Rev. Mod. Phys. **75**, 281 (2003).
[81] W. Paul, Electromagnetic traps for charged and neutral particles, Rev. Mod. Phys. **62**, 531 (1990).
[82] D. J. Wineland, C. Monroe, W. M. Itano, D. Leibfried, B. E. King, and D. M. Meekhof, Experimental issues in coherent quantum-state manipulation of trapped atomic ions, J. Res. Natl. Inst. Stand. Technol. **103**, 259 (1998).
[83] N. Šibalić, J. D. Pritchard, C. S. Adams, and K. J. Weatherill, ARC: An open-source library for calculating properties of alkali Rydberg atoms, Comput. Phys. Commun. **220**, 319 (2017).
[84] M. A. Simón, M. Palmero, S. Martínez-Garaot, and J. G. Muga, Trapped-ion Fock-state preparation by potential deformation, Phys. Rev. Res. **2**, 023372 (2020).
[85] L. S. Brown and G. Gabrielse, Geonium theory: Physics of a single electron or ion in a Penning trap, Rev. Mod. Phys. **58**, 233 (1986).
[86] W. M. Itano, J. C. Bergquist, J. J. Bollinger, and D. J. Wineland, Cooling methods in ion traps, Phys. Scr. **1995**, 106 (1995).
[87] D. J. Gorman, P. Schindler, S. Selvarajan, N. Daniilidis, and H. Häffner, Two-mode coupling in a single-ion oscillator via parametric resonance, Phys. Rev. A **89**, 062332 (2014).
[88] C. Zener and R. H. Fowler, Non-adiabatic crossing of energy levels, Proc. R. Soc. A **137**, 696 (1932).
[89] C. Wittig, The Landau-Zener formula, J. Phys. Chem. B **109**, 8428 (2005).
[90] M. N. Gaboriaud, M. Desaintfuscien, and F. G. Major, Absolute measurement of the total number of ions stored in an RF quadrupole trap, Int. J. Mass Spectrom. Ion Phys. **41**, 109 (1981).
[91] H. Dehmelt, Continuous Stern-Gerlach effect: Principle and idealized apparatus, Proc. Natl. Acad. Sci. U.S.A. **83**, 2291 (1986).
[92] J. Tan and G. Gabrielse, Synchronization of parametrically pumped electron oscillators with phase bistability, Phys. Rev. Lett. **67**, 3090 (1991).
[93] N. Yu, H. Dehmelt, and W. Nagourney, Noise-free parametric energy multiplication for frequency measurements of an anharmonic mono-ion oscillator, J. Appl. Phys. **73**, 8650 (1993).
[94] M. Brownnutt, M. Kumph, P. Rabl, and R. Blatt, Ion-trap measurements of electric-field noise near surfaces, Rev. Mod. Phys. **87**, 1419 (2015).
[95] J. A. Sedlacek, J. Stuart, D. H. Slichter, C. D. Bruzewicz, R. McConnell, J. M. Sage, and J. Chiaverini, Evidence for multiple mechanisms underlying surface electric-field noise in ion traps, Phys. Rev. A **98**, 063430 (2018).
[96] Y. Chu, S. Zhang, B. Yu, and J. Cai, Dynamic framework for criticality-enhanced quantum sensing, Phys. Rev. Lett. **126**, 010502 (2021).
[97] G. Koolstra, G. Yang, and D. I. Schuster, Coupling a single electron on superfluid helium to a superconducting resonator, Nat. Commun. **10**, 5323 (2019).
[98] X. Zhou, G. Koolstra, X. Zhang, G. Yang, X. Han, B. Dizdar, X. Li, R. Divan, W. Guo, K. W. Murch, D. I. Schuster, and D. Jin, Single electrons on solid neon as a solid-state qubit platform, Nature (London) **605**, 46 (2022).
[99] X. Zhou, X. Li, Q. Chen, G. Koolstra, G. Yang, B. Dizdar, Y. Huang, C. S. Wang, X. Han, X. Zhang, D. I. Schuster, and D. Jin, Electron charge qubits with 0.1 millisecond coherence time, arXiv:2210.12337.
[100] E. Kawakami, J. Chen, M. Benito, and D. Konstantinov, Blueprint for quantum computing using electrons on helium, Phys. Rev. Appl. **20**, 054022 (2023).
[101] D. An, A. M. Alonso, C. Matthiesen, and H. Häffner, Coupling two laser-cooled ions via a room-temperature conductor, Phys. Rev. Lett. **128**, 063201 (2022).
[102] M. Bohman, V. Grunhofer, C. Smorra, M. Wiesinger, C. Will, M. J. Borchert, J. A. Devlin, S. Erlewein, M. Fleck, S. Gavranovic, J. Harrington, B. Latacz, A. Mooser, D. Popper, E. Wursten, K. Blaum, Y. Matsuda, C. Ospelkaus, W. Quint, J. Walz, and S. Ulmer, Sympathetic cooling of a trapped proton mediated by an LC circuit, Nature (London) **596**, 514 (2021).